Opto-Electronic Advances

Original Article

2021, Vol. 4, No. 5

DOI: 10.29026/oea.2021.200006

Switchable diurnal radiative cooling by doped VO_2

Minkyung Kim[1†], Dasol Lee[1†], Younghwan Yang[1] and Junsuk Rho[1,2*]

This paper presents design and simulation of a switchable radiative cooler that exploits phase transition in vanadium dioxide to turn on and off in response to temperature. The cooler consists of an emitter and a solar reflector separated by a spacer. The emitter and the reflector play a role of emitting energy in mid-infrared and blocking incoming solar energy in ultraviolet to near-infrared regime, respectively. Because of the phase transition of doped vanadium dioxide at room temperature, the emitter radiates its thermal energy only when the temperature is above the phase transition temperature. The feasibility of cooling is simulated using real outdoor conditions. We confirme that the switchable cooler can keep a desired temperature, despite change in environmental conditions.

Keywords: phase change material; photonic crystal; passive thermoregulation; switchable radiative cooling; Fabry-Pérot resonance

Kim MK, Lee DS, Yang YH, Rho JS. Switchable diurnal radiative cooling by doped VO_2. *Opto-Electron Adv* **4**, 200006 (2021).

Introduction

Every object with finite temperature emits heat by thermal radiation. If an object radiates more energy than it absorbs from its surroundings, it loses energy and cools down. This phenomenon occurs generally at night when the object is not subject to solar irradiation, and forms a basis of nocturnal radiative cooling[1–3]. However, it has been recently suggested that a material that reflects solar energy but radiates in an atmospheric window (wavelengths 8 μm< λ < 13 μm) can lose energy during the day[4]. This observation has stimulated studies on diurnal radiative cooling, in which an object can cool down even under solar illumination without consuming external energy[5–9]. Therefore, diurnal radiative cooling has been evaluated as an alternative cooling technology for future.

For efficient radiative cooling, two conditions should be satisfied. The absorptivity of the object should be near zero in the ultraviolet (UV) to near-infrared (NIR) range, and should radiate its energy with near-unity efficiency in the wavelengths at which electromagnetic radiation can be transmitted through the atmosphere (the "atmospheric window"). To meet those conditions, structured materials such as photonic crystals[10], micro/nanoporous structures[11–17], multilayer[18,19], and mixtures of dielectric particles[20–23] have been used for their ability to manipulate optical responses. However, the spectra of such media cannot be changed after fabrication. Therefore, many efforts have been devoted to find optical materials and structures that have switchable thermal characteristics.

An interesting example is the use of vanadium dioxide (VO_2). It is a phase change material that has an insulating phase at temperature T below the critical temperature T_c and metallic phase at $T > T_c$. The phase

[1]Department of Mechanical Engineering, Pohang University of Science and Technology (POSTECH), Pohang 37673, Republic of Korea; [2]Department of Chemical Engineering, Pohang University of Science and Technology (POSTECH), Pohang 37673, Republic of Korea.

†These authors contributed equally to this work.

*Correspondence: JS Rho, E-mail: jsrho@postech.ac.kr

Received: 28 February 2020; Accepted: 22 June 2020; Published: 20 May 2021

transition of VO_2 has been used to develop active emitters and absorbers[24–26], switchable polarization rotators[27], waveguides[28] and nanoantennas[29]. T_c of pure VO_2 is 68 °C, but can be set to around room temperature by doping molybdenum, tungsten and/or strontium[30–37] and by growing VO_2 thin film on TiO_2 substrates[38,39]. This relatively low T_c of VO_2 encouraged the development of an active radiative cooler[40] based on the transmissive filter placed on a switchable emitter and a photonic-based thermostat[41] consisting of repeated layers of VO_2 grown on TiO_2 film and zinc selenide. Such active thermal devices radiate only at $T > T_c$ and thus lose their thermal energies as temperature increases while maintaining temperature similar to ambient as temperature decreases. Here, we develop a switchable radiative cooler by combining two parts: an emitter that uses doped VO_2, and a solar reflector that has optimized one-dimensional multi-stacked photonic crystals. The emitter part is designed to selectively radiate in the atmospheric window whereas the solar reflector blocks solar irradiance in UV to NIR regime. Thus, the cooler exhibits positive cooling power at $T > T_c$ and negative cooling power at $T < T_c$. Therefore, it maintains a moderate temperature that is resilient to environmental changes. Simulation using a diurnal cycle of outdoor temperature and solar radiation proved that the radiative cooler is capable of switchable diurnal radiative cooling. In comparison to other static radiative cooler, the switchable radiative cooler exhibits minimal variation of temperature, and is therefore useful in various applications including air conditioning and heating.

Results and discussion

Material properties and design

The optical behavior of VO_2 can be described as Fig. 1(a). In the infrared range, VO_2 responses as a metal well above T_c and as an insulator well below T_c. To avoid an unphysical result, we assume that the permittivity of VO_2 changes continuously and smoothly in a narrow transition range $[T_c - \Delta T, T_c + \Delta T]$. Thus, the permittivity of VO_2 is modelled individually in three distinct regimes: insulating, transition and metallic regime (Fig. 1(a)). For insulating and metallic regime, we use permittivities of doped VO_2 presented in ref.[40]. In the transition regime, we assume that permittivity changes as an arctan function (Fig. 1(b)):

$$\varepsilon_{\text{transition}} = \arctan\left(\frac{T - T_c}{\Delta T} \times 10\right) \times \frac{\varepsilon_m - \varepsilon_i}{2\arctan 10} + \frac{\varepsilon_m + \varepsilon_i}{2}\ , \tag{1}$$

where ε_m and ε_i are permittivity in the metallic and insulating phase, respectively. Throughout this paper, we

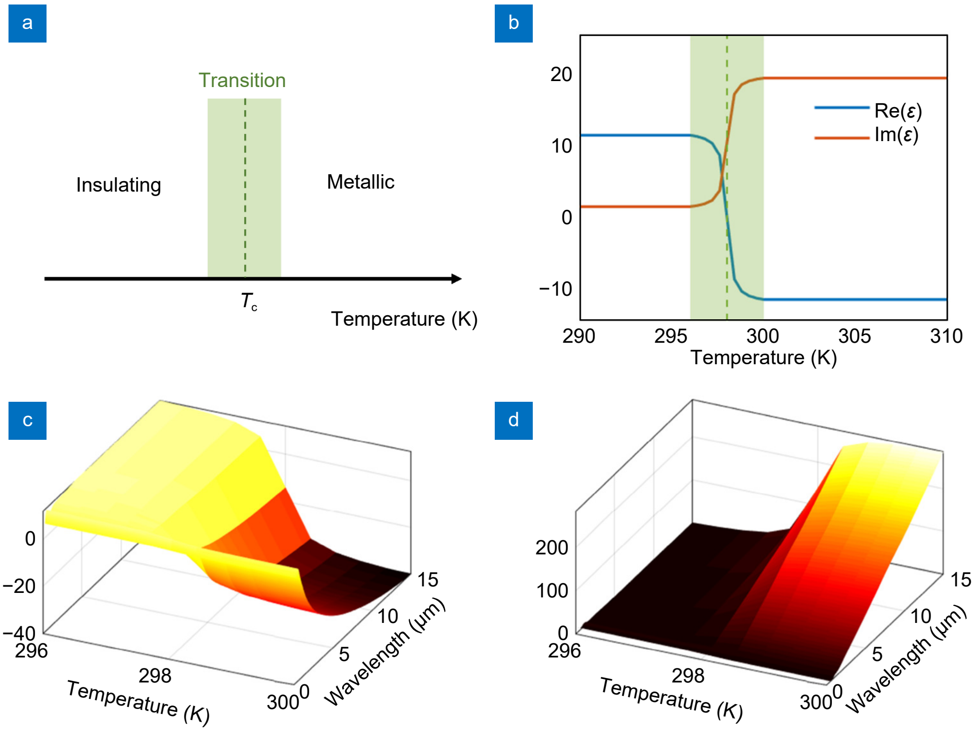

Fig. 1 | Temperature-dependent material responses of VO_2. (**a**) Schematic of temperature-dependent phase. (**b**) Permittivity at 2 μm when T_c = 298 K. Shaded area represents transition regime. (**c**) Real and (**d**) imaginary part of permittivity in transition regime.

set T_c = 298 K and ΔT = 2 K. In the transition regime, both the real and imaginary parts of $\varepsilon_{transition}$ change smoothly (Figs. 1(c) and 1(d)).

To minimize the absorption of solar irradiance and maximize thermal energy radiated through the atmospheric window in a switchable way, we combine an emitter and a solar reflector separated by a spacer (Fig. 2) on a SiO_2 substrate. The emitter part is composed of stacked layers of silver (200 nm), silicon (700 nm) and VO_2 (10 nm) from bottom to top. A 300 nm-thick spacer made of poly(methyl methacrylate) (PMMA) is deposited on the emitter. The top of the spacer is the solar reflector consisting of three stacked photonic crystals. Each photonic crystal (PC_i) is a distributed Bragg reflector (DBR) that is designed to suppress absorption at a target wavelength λ_i where λ_1 = 0.52 μm, λ_2 = 0.76 μm and λ_3 = 1.18 μm. Thickness of each layer is set as $\lambda_i/4n$ following the design rule of DBRs[42].

Optical responses

The transfer-matrix method was used to calculate the absorptivity and reflectivity spectra[43]. We examine absorptivity and reflectivity of the emitter part and solar reflector part individually. The emitter works as a metal-insulator-metal structure at $T > T_c$. The Fabry-Pérot resonance due to the cavity results in high absorptivity near the atmospheric window (Fig. 3(a)). In contrast, the emitter behaves as an insulator deposited on a metal and mostly reflects at $T < T_c$ (Fig. 3(b)). Therefore, the emitter performs the switching of radiation in the atmospheric window. Meanwhile, the solar reflector reflects solar irradiance in the UV to NIR range (Fig. 3(c)). The high reflectivity of the solar reflector originates from the optimization of photonic crystal structures. The average absorptivity of the solar reflector at λ < 2 μm is 5.9 %. The combined structure of emitter separated by a spacer from the solar reflector has low absorption in UV to NIR

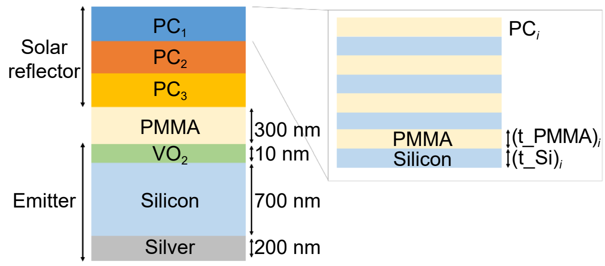

Fig. 2 | Design of the switchable radiative cooler. Emitter part consists of stacked layers of silver, silicon and VO_2. Solar reflector part consists of three photonic crystals that have 4 pairs of PMMA and silicon. PC_i is designed to suppress absorption at λ_i where λ_1 = 0.52 μm, λ_2 = 0.76 μm and λ_3 = 1.18 μm. Thickness of each layer is $\lambda_i/4n$.

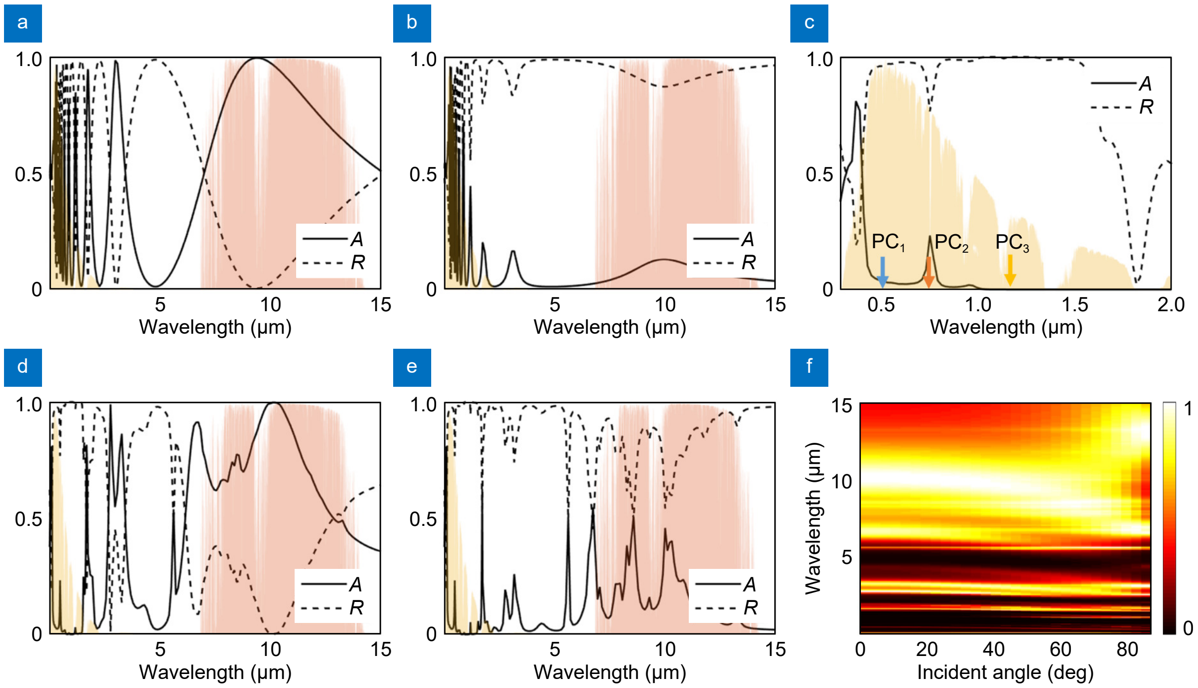

Fig. 3 | Absorptivity and reflectivity of the switchable radiative cooler. (**a**, **b**) Absorptivity and reflectivity of the emitter part when VO_2 is in (a) metallic and (b) insulating state. (**c**) Absorptivity and reflectivity of the solar reflector part. Three arrows represent the target wavelengths of three photonic crystals. (**d**, **e**) Absorptivity and reflectivity of the switchable radiative cooler when VO_2 is in (d) metallic and (e) insulating state. Incident angle is zero. (**f**) Absorptivity of the switchable radiative cooler when VO_2 is metallic.

and switchable absorption in the atmospheric window simultaneously. Absorptivity in UV to NIR is low in both metallic and insulating phases; the combined structure absorbs 7.6 % in average. In contrast, absorptivity in the atmospheric window are remarkably distinct in two phases. The absorptivity is high in the metallic phase, but low in the insulating phase (Figs. 3(d) and 3(e)). Average absorptivity is 78 % in the metallic phase and 18 % in the insulating phase. At oblique incidence, the absorptivity remains high in the atmospheric window (Fig. 3(f)).

Calculation of cooling flux

To evaluate the cooling flux, we consider blackbody radiation, solar irradiance, thermal exchange with atmosphere, and two other heat exchange channels[4]:

$$P(T) = P_{\rm rad}(T) - P_{\rm sun} - P_{\rm atm}(T_{\rm amb}) - P_{\rm cc}(T, T_{\rm amb}) \ , \tag{2}$$

where T is the temperature of the switchable radiative cooler, $T_{\rm amb}$ is ambient temperature, and $P_{\rm rad}(T)$ corresponds to radiation flux emitted by the cooler:

$$P_{\rm rad}(T) = \iint_0^\infty I_{\rm BB}(T,\lambda)E(T,\lambda,\theta){\rm d}\lambda\cos\theta{\rm d}\Omega \ , \tag{3}$$

where λ is the wavelength, θ is the polar angle, and $\int {\rm d}\Omega = 2\pi\int_0^{\pi/2}\sin\theta{\rm d}\theta$ is the angular integral over a hemisphere. E is the emissivity of the cooler and is equal to the absorptivity according to Kirchhoff's law[44]. Since E of VO_2 depends on its temperature, we use $E(T, \lambda, \theta)$ instead of $E(\lambda, \theta)$.

$$I_{\rm BB}(T,\lambda) = \frac{2{\rm h}c^2}{\lambda^5}\frac{1}{{\rm e}^{{\rm h}c/(\lambda k_{\rm B}T)}-1} \ , \tag{4}$$

is the spectral radiance density of a blackbody at temperature T, where h is Planck constant, c is the speed of light in free space, and $k_{\rm B}$ is the Boltzmann constant. The second term represents absorbed thermal flux due to solar irradiance:

$$P_{\rm sun} = \int_0^\infty E(T,\lambda)I_{\rm AM1.5}(\lambda)\,{\rm d}\lambda \ , \tag{5}$$

where $I_{\rm AM1.5}$ is the AM1.5 spectrum of the solar illumination. Thermal flux absorbed by the atmospheric heat exchange is

$$P_{\rm atm}(T_{\rm amb}) = \iint_0^\infty I_{\rm BB}(T_{\rm amb},\lambda)E(T,\lambda,\theta) \cdot E_{\rm atm}(\lambda,\theta){\rm d}\lambda\cos\theta{\rm d}\Omega \ , \tag{6}$$

where $E_{\rm atm} = 1 - t(\lambda)^{1/\cos\theta}$ is the emissivity of the atmosphere where $t(\lambda)$ is the transmittance of the atmosphere in the zenith direction[1,45]. The last term is associated with conduction and convection given as

$$P_{\rm cc}(T, T_{\rm amb}) = h_{\rm cc}(T_{\rm amb} - T) \ , \tag{7}$$

where $h_{\rm cc}$ is the heat transfer coefficient due to conduction and convection. We use $h_{\rm cc}$ = 6.9 $\rm Wm^{-2}K^{-1}$ throughout the calculations.

The cooling flux $P(T)$ under normal incidence of solar energy is calculated using Eq. (2) to (7). For simplification, we first treat E as a temperature-independent value. We calculate the cooling flux of the cooler by assuming that VO_2 is either metallic or insulating regardless of temperature (Fig. 4(a)). When VO_2 is assumed to be metallic, it has positive cooling flux above T = 297.8 K and negative cooling flux below it. As expected, the cooling flux when VO_2 is insulating is lower than that when it is metallic. The cooling flux is zero at T = 306 K for the insulating case.

In reality, E of VO_2 varies with T and thus, E should be treated as a function of temperature. Cooling flux is expected to be equal to that of metallic case at $T > T_c + \Delta T$ and to that of insulating case at $T < T_c - \Delta T$. In the vicinity of T_c, it is assumed to change continuously and smoothly. We use Eq. (1) to calculate emissivity of the radiative cooler, then obtain the cooling flux in the transition regime when $T_{\rm amb}$ = 303 K (Fig. 4(b)). The cooling flux varies by amount of more than 100 $\rm Wm^{-2}$

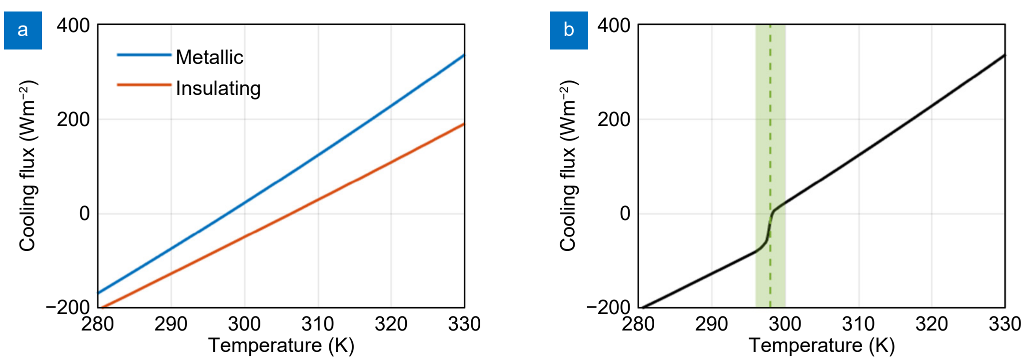

Fig. 4 | Cooling flux of the radiative cooler under normal incidence of solar energy when $T_{\rm amb}$ = 303 K. (**a**, **b**) Cooling flux when permittivity of VO_2 is assumed to be (a) static and (b) dynamic. Shaded area represents the transition regime.

across the transition regime. In the atmospheric window, the cooler radiates approximately P_{rad} = 179 Wm^{-2} when the cooling is turned on ($T = T_c + \Delta T$) and P_{rad} = 47 Wm^{-2} when the cooling is turned off ($T = T_c - \Delta T$). The switchable radiative cooler is in thermal equilibrium at T = 298.3 K, which corresponds to room temperature.

Numerical observation of cooling in time

To confirm the cooling visually, we calculate how temperature of the switchable radiative cooler changes over time. Temperature variation obeys the thermal balance equation:

$$C\frac{dT}{dt} = AP(T, T_{amb}) \ , \tag{8}$$

where A is the area of the cooling surface, and t is time. C is the heat capacitance, which can be obtained by summing the heat capacitances of all layers as

$$C = A\sum_j c_j\rho_j t_j + C_0 \ , \tag{9}$$

where c_j, ρ_j and t_j is the specific heat, density and thickness of j-th layer, respectively. The summation applies to layers shown in Fig. 2 and a substrate of 500 μm-thick silicon dioxide (SiO_2). The specific heat and density (Table 1) are obtained from ref.[46,47] for PMMA, ref.[48,49] for silicon, ref.[48,50] for silver, ref.[48,51] for SiO_2, and ref.[52,53] for VO_2. Strictly, specific heat of VO_2 depends on its temperature, but we use the specific heat at room temperature because the variation range is small (< 3 $Jg^{-1}K^{-1}$). To test the cooling ability, we additionally include C_0 = 1.325×10^5 JK^{-1} as the heat capacitance of an object to be cooled; it corresponds to a block of SiO_2 of unit area and 0.05 m thickness.

Table 1 | Specific heat and density of materials.

	PMMA	Silicon	Silver	SiO_2	VO_2
c (J/gK)	1.47	0.71	0.23	1.00	0.24
ρ (g/cm^{-3})	1.18	2.33	10.50	2.65	4.57

We simulate temperature variation in time under T_{amb} = 303 K by using Eq. (2) and Eq. (9). For various initial temperature ranging from 280 K to 320 K, temperature converges to 298.3 K (Fig. 5(a)). It shows that the cooler is turned on at T > 298.3 K but turned off at T < 298.3 K. The switchable cooling is also confirmed by cooling flux which is positive at T > 298.3 K and negative at T < 298.3 K (Fig. 5(b)). The thermal equilibrium temperature can be tuned by designing the solar reflector

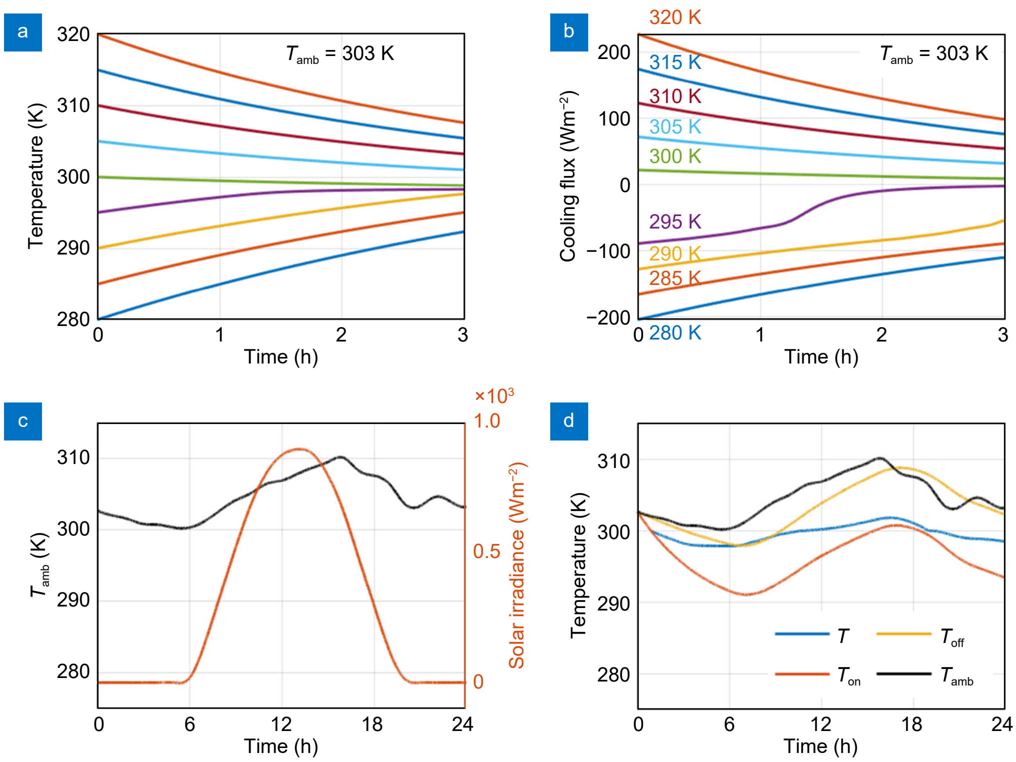

Fig. 5 | Temperature variation in time. (**a**) Temperature and (**b**) cooling flux in time for initial temperature of 280 K to 320 K with 5 K step. Temperature indicate the initial temperature of the cooler. T_{amb} = 303 K. (**c**, **d**) A cycle of temperature of a day. (c) T_{amb} and solar irradiance of July 15, 2018 in Pohang, Korea. (d) Temperature of switchable radiative cooler (blue) and the static radiative cooler when radiative cooling is assumed to be turned on (orange) and off (yellow). T_{amb} is shown as a reference (black). Initial temperature of the cooler is set equal to the initial T_{amb}.

part. Therefore, the switchable radiative cooler provides a pathway to constantly control the temperature at a desired value.

The practicality of the switchable radiative cooler is assessed by simulating a cycle of temperature during a day. To emulate the outdoor condition, we use ambient temperature and solar irradiance I measured on July 15, 2018 in Pohang, Korea by the Korea Meteorological Administration[54] (Fig. 5(c)). Initial temperature of the switchable radiative cooler is set equal to that of ambient. During the whole day, the cooler has $T < T_{amb}$, with the maximum decrement of 8.5 K (Fig. 5(d)). For comparison, we also plot the temperature of the radiative cooler when the cooling is turned on and off at all temperature. In all cases, temperature gets lower before 6 am when the sun rises. When the cooling is turned off, temperature increases as time passes until it reaches the equilibrium and then decreases again after the sunset. On the other hand, when the cooling is turned on, temperature decreases by approximately 10 K as a result of high cooling power. Temperature variation during a day exceeds 10 K in both cases. In contrast, the switchable radiative cooler shows a minimal change of temperature, resilient to the surrounding environment.

Conclusions

In conclusion, we present a switchable radiative cooler made of doped vanadium dioxide. The cooler emits energy in the atmospheric window only above room temperature as a result of Fabry-Pérot resonance. Thus, the cooling is conditionally turned on and off depending on the temperature. We demonstrate the switchable radiative cooling by calculating cooling flux for various temperature ranges. The switchable cooling is further supported by simulating a cycle of temperature for a day using the measured temperature and solar irradiance data. We confirm that the cooler can maintain its temperature robustly under natural weather conditions. To further improve the cooling effect of the switchable diurnal radiative cooler, the design can be optimized to have unity (zero) reflectivity in the UV to NIR range and emissivity in the atmospheric window at $T > T_c$ (at $T < T_c$) or to have the highest cooling flux by various optimization methods and machine learning[55–57]. The switchable radiative cooler will facilitate self-adaptive control of thermal energy and can be implemented in a variety of applications such as passive cooling in environmentally-benign buildings and vehicles.

References

1. Granqvist CG, Hjortsberg A. Radiative cooling to low temperatures: general considerations and application to selectively emitting SiO films. *J Appl Phys* **52**, 4205–4220 (1981).
2. Gentle AR, Smith GB. Radiative heat pumping from the Earth using surface phonon resonant nanoparticles. *Nano Lett* **10**, 373–379 (2010).
3. Catalanotti S, Cuomo V, Piro G, Ruggi D, Silvestrini V et al. The radiative cooling of selective surfaces. *Sol Energy* **17**, 83–89 (1975).
4. Raman AP, Anoma MA, Zhu LX, Rephaeli E, Fan SH. Passive radiative cooling below ambient air temperature under direct sunlight. *Nature* **515**, 540–544 (2014).
5. Huang X, Li N, Wang JF, Liu DF, Xu ZJ et al. Single nanoporous $MgHPO_4\cdot 1.2H_2O$ for daytime radiative cooling. *ACS Appl Mater Interfaces* **12**, 2252–2258 (2020).
6. Ko B, Lee D, Badloe T, Rho J. Metamaterial-based radiative cooling: towards energy-free all-day cooling. *Energies* **12**, 1–14 (2018).
7. Li T, Zhai Y, He SM, Gan WT, Wei ZY et al. A radiative cooling structural material. *Science* **364**, 760–763 (2019).
8. Hsu PC, Song AY, Catrysse PB, Liu C, Peng YC et al. Radiative human body cooling by nanoporous polyethylene textile. *Science* **353**, 1019–1023 (2016).
9. Li W, Fan SH. Nanophotonic control of thermal radiation for energy applications[Invited]. *Opt Express* **26**, 15995–16021 (2018).
10. Kou JL, Jurado Z, Chen Z, Fan SH, Minnich AJ. Daytime radiative cooling using near-black infrared emitters. *ACS Photonics* **4**, 626–630 (2017).
11. Peng YC, Chen J, Song AY, Catrysse PB, Hsu PC et al. Nanoporous polyethylene microfibres for large-scale radiative cooling fabric. *Nat Sustain* **1**, 105–112 (2018).
12. Mandal J, Fu YK, Overvig AC, Jia MX, Sun KR et al. Hierarchically porous polymer coatings for highly efficient passive daytime radiative cooling. *Science* **362**, 315–319 (2018).
13. Cai LL, Song AY, Wu PL, Hsu PC, Peng YC et al. Warming up human body by nanoporous metallized polyethylene textile. *Nat Commun* **8**, 496 (2017).
14. Yang AK, Cai LL, Zhang RF, Wang JY, Hsu PC et al. Thermal management in nanofiber-based face mask. *Nano Lett* **17**, 3506–3510 (2017).
15. Lee D, Go M, Son S, Kim M, Badloe T et al. Sub-ambient daytime radiative cooling by silica-coated porous anodic aluminum oxide. *Nano Energy* **79**, 105426 (2021).
16. Heo SY, Lee GJ, Kim DH, Kim YJ, Ishii S et al. A Janus emitter for passive heat release from enclosures. *Sci Adv* **6, 36**, eabb1906 (2020).
17. Lee GJ, Kim DH, Heo SY, Song YM. Spectrally and spatially selective emitters using polymer hybrid spoof plasmonics. *ACS Appl Mater Interfaces* **12, 47**, 53206–53214 (2020).
18. Kim M, Lee D, Son S, Yang Y, Lee H et al. Visibly transparent radiative cooler under direct sunlight. *Adv Opt Mater* , 2002226 (2021).
19. Chae D, Kim M, Jung PH, Son S, Seo J et al. Spectrally selective inorganic-based multilayer emitter for daytime radiative cooling. *ACS Appl Mater Interfaces* **12, 7**, 8073–8081 (2020).
20. Atiganyanun S, Plumley JB, Han SJ, Hsu K, Cytrynbaum J et al. Effective radiative cooling by paint-format microsphere-based photonic random media. *ACS Photonics* **5**, 1181–1187 (2018).
21. Bao H, Yan C, Wang BX, Fang X, Zhao CY et al. Double-layer

nanoparticle-based coatings for efficient terrestrial radiative cooling. *Sol Energ Mater Sol C* **168**, 78–84 (2017).
22. Huang ZF, Ruan XL. Nanoparticle embedded double-layer coating for daytime radiative cooling. *Int J Heat Mass Transf* **104**, 890–896 (2017).
23. Zhai Y, Ma YG, David SN, Zhao DL, Lou RN et al. Scalable-manufactured randomized glass-polymer hybrid metamaterial for daytime radiative cooling. *Science* **355**, 1062–1066 (2017).
24. Nishikawa K, Yatsugi K, Kishida Y, Ito K. Temperature-selective emitter. *Appl Phys Lett* **114**, 211104 (2019).
25. Chen MK, Morsy AM, Povinelli ML. Design of VO_2-coated silicon microspheres for thermally-regulating paint. *Opt Express* **27**, 21787–21793 (2019).
26. Long LS, Taylor S, Ying XY, Wang LP. Thermally-switchable spectrally-selective infrared metamaterial absorber/emitter by tuning magnetic polariton with a phase-change VO_2 layer. *Mater Today Energy* **13**, 214–220 (2019).
27. Jia ZY, Shu FZ, Gao YJ, Cheng F, Peng RW et al. Dynamically switching the polarization state of light based on the phase transition of vanadium dioxide. *Phys Rev Appl* **9**, 034009 (2018).
28. Markov P, Marvel RE, Conley HJ, Miller KJ, Haglund Jr RF et al. Optically monitored electrical switching in VO_2. *ACS Photonics* **2**, 1175–1182 (2015).
29. Shu FZ, Zhang LH, Wang JN, Peng RW, Fan RH et al. Dynamically tunable bowtie nanoantennas based on the phase transition of vanadium dioxide. *Opt Lett* **44**, 2752–2755 (2019).
30. Dietrich MK, Kuhl F, Polity A, Klar PJ. Optimizing thermochromic VO_2 by co-doping with W and Sr for smart window applications. *Appl Phys Lett* **110**, 141907 (2017).
31. Burkhardt W, Christmann T, Franke S, Kriegseis W, Meister D et al. Tungsten and fluorine co-doping of VO_2 films. *Thin Solid Films* **402**, 226–231 (2002).
32. Jorgenson GV, Lee JC. Doped vanadium oxide for optical switching films. *Sol Energy Mater* **14**, 205–214 (1986).
33. Wang XJ, Liu YY, Li DH, Feng BH, He ZW et al. Structural and optical properties of tungsten-doped vanadium dioxide films. *Chin Phys B* **22**, 066803 (2013).
34. Zhang YF, Zhang JC, Zhang XZ, Huang C, Zhong YL et al. The additives W, Mo, Sn and Fe for promoting the formation of VO_2(M) and its optical switching properties. *Mater Lett* **92**, 61–64 (2013).
35. Liu SJ, Fang HW, Su YT, Hsieh JH. Metal–insulator transition characteristics of Mo- and Mn-doped VO_2 films fabricated by magnetron cosputtering technique. *Jpn J Appl Phys* **53**, 063201 (2014).
36. Khan GR, Asokan K, Ahmad B. Room temperature tunability of Mo-doped VO_2 nanofilms across semiconductor to metal phase transition. *Thin Solid Films* **625**, 155–162 (2017).
37. Rajeswaran B, Umarji AM. Effect of W addition on the electrical switching of VO_2 thin films. *AIP Adv* **6**, 035215 (2016).
38. Muraoka Y, Hiroi Z. Metal–insulator transition of VO_2 thin films grown on TiO_2 (001) and (110) substrates. *Appl Phys Lett* **80**, 583–585 (2002).
39. Fan LL, Chen S, Luo ZL, Liu QH, Wu YF et al. Strain dynamics of ultrathin VO_2 film grown on TiO_2 (001) and the associated phase transition modulation. *Nano Lett* **14**, 4036–4043 (2014).
40. Ono M, Chen KF, Li W, Fan SH. Self-adaptive radiative cooling based on phase change materials. *Opt Express* **26**, A777–A787 (2018).
41. Kort-Kamp WJM, Kramadhati S, Azad AK, Reiten MT, Dalvit DAR. Passive radiative "thermostat" enabled by phase-change photonic nanostructures. *ACS Photonics* **5**, 4554–4560 (2018).
42. Hecht E. *Optics* (Pearson Higher Education, Harlow, 2017).
43. Yeh P. *Optical Waves in Layered Media* 95 (Wiley Online Library, New York, 1988).
44. Kirchhoff G. Ueber das Verhältniss zwischen dem Emissionsvermögen und dem Absorptionsvermögen der Körper für Wärme und Licht. *Ann Phys* **185**, 275–301 (1860).
45. Berk A, Anderson GP, Acharya PK, Bernstein LS, Muratov L et al. MODTRAN5: 2006 update. *Proc SPIE* **6233**, 62331F (2006).
46. Brandrup J, Immergut EH. *Polymer Handbook* 2nd ed (John Wiley and Sons, London, 1975).
47. Wypych G. PMMA polymethylmethacrylate. *Handbook of Polymers* 2nd ed 450–454 (Elsevier, Oxford, 2012).
48. Haynes WM, Lide DR, Bruno TJ. *CRC Handbook of Chemistry and Physics* (CRC Press, Boca Raton, 2014).
49. Dargys A, Kundrotas J. *Handbook on Physical Properties of Ge, Si, GaAs and InP* (Science and Encyclopedia Publ., Vilniys, 1994).
50. Tipler PA, Mosca G. *Physics for Scientists and Engineers* 6th ed (WH Freeman, 2007).
51. Grove AS. *Physics and Technology of Semiconductor Devices* (Wiley, New York, 1967).
52. National Center for Biotechnology Information. PubChem Database. Vanadium dioxide, CID=82849. https://pubchem.ncbi.nlm.nih.gov/compound/Vanadium-dioxide.
53. Chase Jr MW. *NIST-JANAF Thermochemical Tables* 4th ed (American Chemical Society and American Institute of Physics, New York, 1998).
54. Korea Meteorological Administration (ASOS). https://data.kma.go.kr/resources/html/en/aowdp.html.
55. Shi Y, Li W, Raman A, Fan SH. Optimization of multilayer optical films with a memetic algorithm and mixed integer programming. *ACS Photonics* **5**, 684–691 (2018).
56. Chae D, Kim M, Jung PH, Son S, Seo J et al. Spectrally selective inorganic-based multilayer emitter for daytime radiative cooling. *ACS Appl Mater Interfaces* **12**, 8073–8081 (2020).
57. Naghshine BB, Saboonchi A. Optimized thin film coatings for passive radiative cooling applications. *Opt Commun* **410**, 416–423 (2018).

Acknowledgements

This work was financially supported by the Green Science program funded by POSCO, and the National Research Foundation (NRF) grants (NRF-2019R1A2C3003129, CAMM-2019M3A6B3030637, NRF-2019R1A5A8080290, and NRF-2018M3D1A1058997) funded by the Ministry of Science and ICT, Republic of Korea. M. Kim acknowledges the Global Ph.D. fellowship (NRF-2017H1A2A1043204) from the Ministry of Education, Republic of Korea. D. Lee acknowledges the PIURI fellowship funded by POSTECH. Y. Yang acknowledges a fellowship from Hyundai Motor *Chung Mong-Koo* Foundation.

Author contributions

M. K. Kim and D. S. Lee contributed equally to this work. J. S. Rho, M. K. Kim and D. S. Lee conceive the idea and initiate the project. M. K. Kim and D. S. Lee designed the system, performed numerical simulation and wrote manuscript. M. K. Kim and Y. H. Yang analyzed the data. All authors read and approved the final manuscript. J. S. Rho guided the entire work.

Competing interests

The authors declare no competing financial interests.